ISSN 0021-3640, JETP Letters, 2014, Vol. 99, No. 5, pp. 290–294. © Pleiades Publishing, Inc., 2014.
Original Russian Text © Z.D. Kvon, K.M. Dantscher, C. Zoth, D.A. Kozlov, N.N. Mikhailov, S.A. Dvoretsky, S.D. Ganichev, 2014, published in Pis'ma v Zhurnal Eksperimental'noi i Teoreticheskoi Fiziki, 2014, Vol. 99, No. 5, pp. 333–338.

Terahertz Electron Transport in a Two-Dimensional Topological Insulator in a HgTe Quantum Well

Z. D. Kvon[a, b], K. M. Dantscher[c], C. Zoth[c], D. A. Kozlov[a, b, *], N. N. Mikhailov[a, b], S. A. Dvoretsky[a], and S. D. Ganichev[c]

[a] *Rzhanov Institute of Semiconductor Physics, Siberian Branch, Russian Academy of Sciences, Novosibirsk, 630090 Russia*
* *e-mail: dimko@isp.nsc.ru*
[b] *Novosibirsk State University, Novosibirsk, 630090 Russia*
[c] *Terahertz Center, University of Regensburg, 93040 Regensburg, Germany*

Received February 4, 2014

The terahertz response of a two-dimensional topological insulator in a HgTe quantum well to radiation with wavelengths of 118 and 184 μm is investigated. It is found that the photoconductivity is rather high (up to a few percent of dark conductivity) and is manifested in both the local and nonlocal responses of the system. This fact proves that the observed photoconductivity is caused by changes in the transport via edge current-carrying states. The sign and nonresonant character of the photoconductivity indicate that it is caused by the heating of electrons in the system. The analysis of experimental results makes it possible to suggest that this heating originates from the Drude absorption of terahertz radiation by metallic "droplets" appearing owing to fluctuations in the impurity potential and the gap and located in direct proximity to edge states.

DOI: 10.1134/S0021364014050130

The two-dimensional topological insulator in HgTe quantum wells with an inverted band spectrum represents the most remarkable experimental implementation of a topological insulator to date [1, 2]. However, all experimental studies of this system carried out by now have been restricted to its transport response [3–7]. Meanwhile, it is evident that studying the effect of terahertz radiation on this system may both lead to the broadening of the scope of phenomena related to two-dimensional topological insulators and make it possible to obtain new valuable information on their energy spectrum. This possibility stems primarily from the fact that all characteristic energies in the experimentally investigated structures (bulk gap, spacing between the Dirac branches, etc.) lie in the energy range of 5–30 meV, i.e., in the terahertz frequency range.

Here, we investigate for the first time the terahertz response of a two-dimensional topological insulator. The experimental samples were fabricated on the basis of 8.3-nm-thick HgTe quantum wells grown by molecular-beam epitaxy as was described in [8]. The samples represented four-terminal structures with a special crosslike configuration coated with a semitransparent gate (see Fig. 1a). This configuration enables measurements of both photoresistance and photovoltage with negligible contributions from contact regions. Four samples of this kind made from the same wafer were investigated. Their terahertz response (photoconductivity and photovoltage) was measured at wavelengths of 118 and 184 μm in magnetic fields up to 2 T. Submillimeter-wave molecular lasers based on methanol and difluoromethane emitting at 118 and 184 μm, respectively, optically pumped by a CO_2 laser [9, 10] were used as the radiation sources. In both cases, the power of the terahertz radiation was 80–100 mW. Using a pyroelectric camera, we determined that the laser beam has a Gaussian profile with a diameter of about 1.5 mm [11]. The photoconductivity was measured by a conventional modulation technique. The modulation frequency was 30–35 Hz and the dc current fed into the sample was $I = 5$–10 nA.

Let us begin the discussion of the results with the analysis of the transport response of the samples under study. The resistance was measured in the two-terminal (R_{2t}) local configuration (see Fig. 1a), in which the current and potentiometric contacts coincide; in the four-terminal (R_{4t}) quasi-nonlocal configuration, in which different contacts are used for feeding the current and measuring the potential drop; and in the Hall configuration (R_H). Figure 1b shows the dependences of R_{2t} and R_H on the gate voltage V_g for the first sample. The observed behavior is typical of macroscopic two-dimensional topological insulator samples. For gate voltages at which the Fermi level E_F is located in the conduction band, the resistivity is low (on the order of 100 Ω/□). With an increase in the magnitude of the negative gate bias, R_{2t} starts to grow and attains a maximum (which, in this case, is 4 MΩ) at the charge-neutrality point (where the Fermi level crosses the Dirac point). Then, the resistivity decreases, dropping to a few kΩ/□ when the Fermi level appears within the

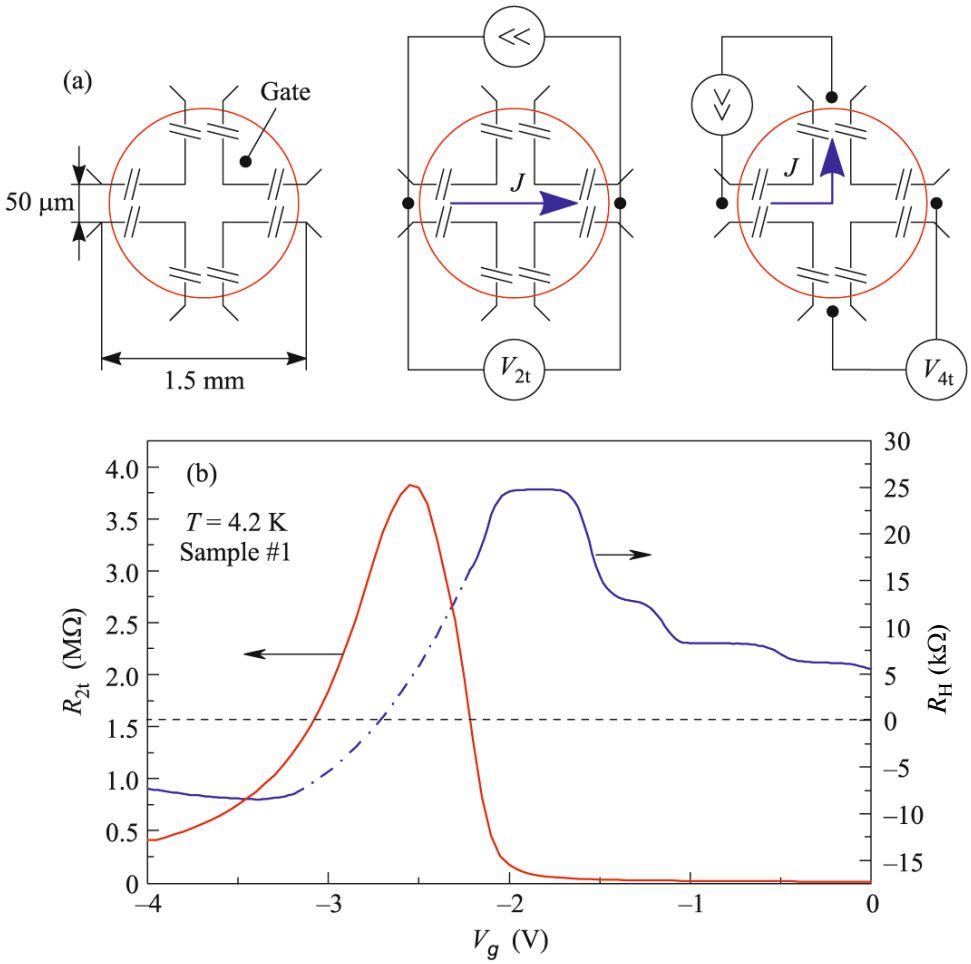

Fig. 1. (Color online) (a) Schematic drawing of the structures under study. The sizes of the structures are shown and different measurement configurations are outlined. (b) Dependences $R_{2t}(V_g)$ for $B = 0$ and $R_H(V_g)$ for $B = 2$ T for the first sample. The part of the $R_H(V_g)$ dependence shown by the dash-dotted line corresponds to the gate-voltage range where measurements of R_H are unreliable (the result of interpolation is shown).

valence band. The $R_H(V_g)$ dependence features well-developed plateaus with $\nu = 1$–4 on the electron side. In the vicinity of the charge-neutrality point, R_H goes through zero, and in the valence band, its sign is reversed.

Figure 2a shows the dependences of $R_{2t}(V_g)$ and the four-terminal (quasi-nonlocal) resistance $R_{4t}(V_g)$ for the second sample under study at temperatures of 2 and 4.2 K. Evidently, the general run of the $R_{2t}(V_g)$ dependence is the same as in Fig. 1b. Thus, similarly to the first sample, we can define three gate-voltage regions for the second sample too. The first region, at low negative voltages ($V_g \geq -1.7$ V), corresponds to the situation where the Fermi level falls within the bulk conduction band; the beginning of this region is labeled as E_c and marked by a vertical arrow. At higher negative voltages, the resistance starts to grow rapidly. This is an indication that the Fermi level has shifted to the bulk gap and charge transport occurs only via edge states. For $V_g = -2.05$ V, both R_{2t} and R_{4t} attain a maximum corresponding to the charge-neutrality point (see Fig. 2a), where the Fermi level coincides with the Dirac point. Then, R_{2t} starts to decrease, but much slower. The latter fact is a result of the longer tail of valence-band states [12]. Finally, for $V_g \leq -2.3$ V, the Fermi level appears in the valence band. Note that the voltages corresponding to E_c and E_v are to some extent arbitrary, because the band edges are broadened owing to disorder.

The positions of the maxima in the dependences $R_{2t}(V_g)$ and $R_{4t}(V_g)$ in Fig. 2a coincide and their ratio is $R_{2t}/R_{4t} = 6.5$. This value exceeds somewhat the one calculated under the assumption of purely edge transport in the vicinity of the charge-neutrality point [5], which is equal to 4. Meanwhile, in the situation where bulk transport is dominant, this ratio should be on the order of 100. This difference is caused by the difference in the current distribution: in the first case, the current is localized near the edge of the sample owing to the existence of the bulk gap, while in the second case it is spread over the entire sample plane. For this reason, in contrast to two-dimensional metals, there is

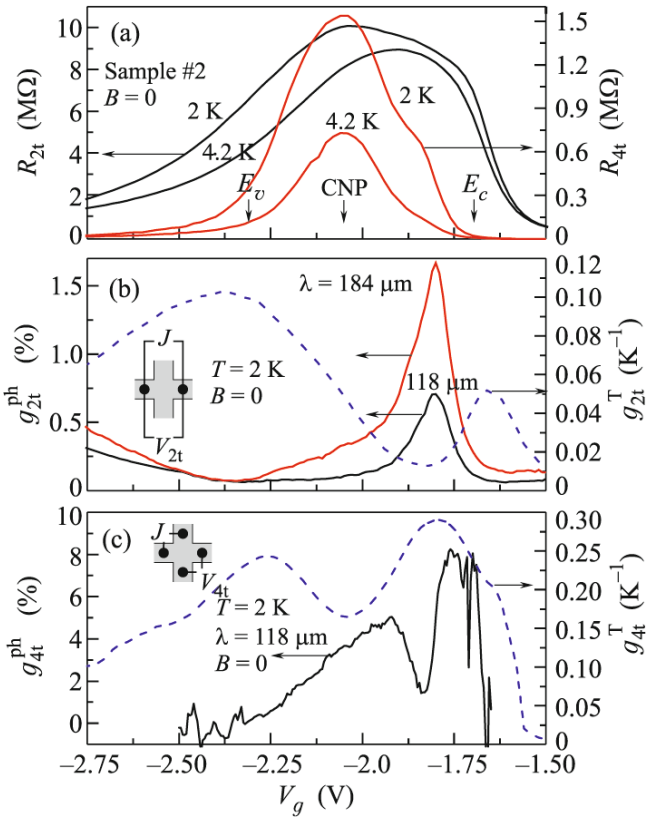

Fig. 2. (Color online) (a) Gate-voltage dependences of the two-terminal resistance $R_{2t}(V_g)$ and quasi-nonlocal (four-terminal) resistance $R_{4t}(V_g)$ at temperatures of 2 and 4.2 K. (b) Gate-voltage dependences of (solid lines) the relative photoconductance $g^{ph}_{2t}(V_g) = \Delta G^{ph}_{2t}/G_{2t}$ for two wavelengths and (dashed line) the relative temperature coefficient of the conductance $g^{T}_{2t} = (dG_{2t}/dT)/G_{2t}$ in the two-terminal configuration. (c) Similar dependences (solid line) $g^{ph}_{4t}(V_g)$ for λ = 118 μm and (dashed line) $g^{T}_{4t}(V_g)$ measured in the quasi-nonlocal (four-terminal) configuration.

no fundamental difference between the resistance measurements in local and nonlocal configurations for the case of the transport response of topological insulators. At the lowest temperature ($T = 2$ K), the ratio R_{2t}/R_{4t} at the maximum of the resistance varies between 4.2 and 8. Noticeable differences may appear both between different samples and between different cooling cycles for the same sample. This may result both from the incomplete "freeze-out" of bulk transport at the lowest temperature in our experiments and from the fact that the ratio $R_{2t}/R_{4t} = 4$ is calculated under the assumption of uniform resistivity of edge channels, which is far from being always true in real samples. The ratio R_{2t}/R_{4t} increases abruptly with deviation from the charge-neutrality point upon variations in the gate voltage and with an increase in temperature. This indicates that the transition from edge to bulk transport takes place. The four-terminal resistance exhibits a more pronounced temperature dependence than the two-terminal resistance owing to the greater sensitivity of the former to shunting by the bulk transport channel. For the same reason, the half-width of the peak in the gate-voltage dependence of R_{4t} is a factor of 2 smaller than that for R_{2t}.

Similarly to two- and four-terminal resistance, we can introduce two- and four-terminal conductance $G_{2(4)t} = 1/R_{2(4)t}$ and photoconductance $\Delta G^{ph}_{2(4)t} = G_{2(4)t} - G^{0}_{2(4)t}$, where $G_{2(4)t}$ and $G^{0}_{2(4)t}$ stand for the two- (four-) terminal conductance of the sample under irradiation and in the dark, respectively. Figure 2b shows typical gate-voltage dependences of the two-terminal relative (i.e., normalized to the total conductance) photoconductance $g^{ph}_{2t}(V_g) = \Delta G^{ph}_{2t}(V_g)/G_{2t}(V_g)$ recorded upon irradiating the sample by terahertz radiation at 118 and 184 μm; the data correspond to the same sample and same measurement cycle as in Fig. 2a. For the convenience of their comparative analysis, Figs. 2a–2c are plotted using the same scale along the V_g axis. Let us discuss the behavior of the relative photoconductance. Evidently, photoconductance is observed at both wavelengths in the entire range of gate voltages—i.e., both when the Fermi level appears within the allowed bulk bands and when it falls within the bulk gap. The magnitude of the photoconductance noticeably varies with V_g in a rather complicated manner. The character of the $g^{ph}_{2t}(V_g)$ dependence is essentially the same for the two wavelengths. When the Fermi level appears within the conduction band ($V_g \geq -1.7$ V), the observed photoconductance is most probably related to the Drude absorption by bulk electrons; evidence of this is the higher magnitude of the photoconductance at 184 μm. When E_F falls within the gap, the photoconductance attains a maximum for $V_g = -1.8$ V, i.e., when E_F appears between the Dirac point and the bottom of the conduction band. With a further increase in the negative bias, g^{ph}_{2t} decreases. At the charge-neutrality point, it is a factor of 3 lower than the peak value. After passing the charge-neutrality point, the photoconductance continues to decrease and attains a minimum at $V_g = -2.3$ V (i.e., in the situation where the Fermi level is about to enter the valence band). As the Fermi level shifts further into the valence band, the photoconductance starts to grow. Note that, in this case, the signal is nearly the same for both wavelengths. This is explained by the fact that the mobility of holes is more than an order of magnitude lower than that of electrons. As a result, $\omega_c \tau^h_p \ll 1$ (where τ^h_p is the hole transport time), and, thus, the frequency dependence of the Drude absorption by holes is negligible.

These data clearly demonstrate that, when the Fermi level falls within the energy range correspond-

ing to the bulk gap, the relative photoconductance in the samples under study is rather large (as large as a few percent at the peak). If the observed photoconductance is caused by the influence of the terahertz radiation on the transport via the edge states, a signal of the same magnitude should also be observed in the quasi-nonlocal configuration. The photoconductance $g_{4t}^{ph}(V_g) = \Delta G_{4t}^{ph}(V_g)/G_{4t}(V_g)$ measured in this configuration is plotted in Fig. 2c. Evidently, the effect is observed in this case as well, and the signal is even much larger (about an order of magnitude) than in the other configuration. Thus, the data shown in Fig. 2 support the conclusion that we have observed for the first time terahertz photoconductance for the two-dimensional topological insulator in HgTe quantum wells. The photoconductance may be fairly large (up to 10%). The comparison of the curves in Figs. 2b and 2c clearly demonstrates that the behaviors of the dependence $g_{4t}^{ph}(V_g)$ are different. The photoconductance at the charge-neutrality point is comparable to the photoconductance corresponding to the location of the Fermi level between the Dirac point and the bottom of the conduction band. Furthermore, the nonlocal photoconductance features two maxima, of which one is close to the charge-neutrality point and the other appears near the bottom of the conduction band.

Next, let us discuss possible mechanisms responsible for the observed photoconductance and analyze some of its features. The photoconductance is positive; i.e., terahertz radiation causes an increase in the conductance of the two-dimensional topological insulator. According to Fig. 2a, the conductance of the samples under study in the vicinity of the charge-neutrality point increases as the temperature is raised from 2 to 4.2 K. Thus, it may be suggested that the observed photoconductance originates from heating. Figures 2b and 2c show the gate-voltage dependences of the relative temperature coefficient of the conductance $g_{4t}^{ph}(V_g) = \Delta G_{4t}^{ph}(V_g)/G_{4t}(V_g)$ and $g_{2t}^{T} = (dG_{2t}/dT)/G_{2t}$ measured in the two-terminal and four-terminal configurations, respectively. Evidently, g_{2t}^{T} is much smaller than g_{4t}^{T}. The same relationship is observed for the photoconductance. This supports the conclusion that the photoconductance is caused by heating. Meanwhile, the gate-voltage dependences of g_{2t}^{T} and g_{4t}^{T} do not coincide with the corresponding dependences of the photoconductance. This fact suggests that the behavior of the photoconductance is determined by the mechanism of the absorption of terahertz radiation. Thus, let us consider the possible mechanisms of terahertz absorption. The energy spectrum of HgTe quantum wells with the inverted spectrum is well known for both (100)- and (013)-oriented structures (see [13] and [14], respectively). In particular, for 8.3-nm-thick quantum wells under study, the bulk gap

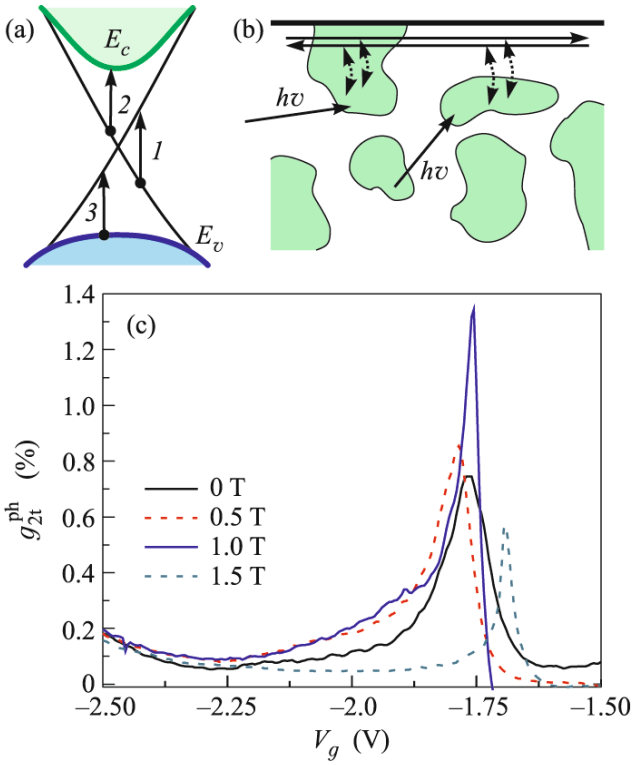

Fig. 3. (Color online) (a) Three possible types of transitions in a two-dimensional topological insulator. (b) Schematic outline of electron "droplets" absorbing terahertz radiation and interacting with one-dimensional edge channels. (c) Dependences $g_{2t}^{ph}(V_g)$ in magnetic fields of 0, 0.5, 1, and 1.5 T at a wavelength of 118 μm at 2 K.

equals 30 meV, which is several times higher than the photon energies for both wavelengths used here ($h\nu$ = 10.6 and 6.7 meV for λ = 118 and 184 μm, respectively). Then, four mechanisms of the absorption of terahertz radiation are possible (see Fig. 3a): (i) transitions between the Dirac branches of the edge states, (ii) transitions between the electron Dirac branch and the conduction band, (iii) transitions between the valence band and the hole Dirac branch, and (iv) Drude absorption. The analysis of absorption resulting from the transitions of the first type demonstrates that electric-dipole transitions between the Dirac branches are forbidden and only much weaker magnetic-dipole transitions are possible [15]. Thus, direct transitions between the Dirac branches can hardly cause a noticeable increase in the electron temperature. Even more important, such transitions would lead to a quasi-resonance behavior of the photoconductance and, thus, to a strong dependence of its peak on the radiation wavelength, completely in contradiction with the experimental results (Fig. 2b). Similar considerations suggest that transitions of the second and third types do not contribute to the observed effect either. Thus, we need to look for another mechanism explaining the observed photoconductance. It is known that ballistic transport in

two-dimensional topological insulators in HgTe structures persists only for characteristic lengths shorter than 1 μm. If these lengths exceed several microns, quantized conductance is not observed anymore [3, 6]. Furthermore, it was recently shown that, in two-dimensional topological insulators with long edges (up to 0.1 mm), there is virtually no increase in resistivity with decreasing temperature even as the temperature is reduced to as low as 100 mK [16]; i.e., there are no indications of one-dimensional localization. A theory explaining such a behavior [17] considers transport along one-dimensional channels extensively exchanging with metallic "droplets" adjacent to the edge of the sample. Such droplets were also observed in scanning tunneling microscopy experiments [18]. Most probably, it is the Drude absorption by these droplets that causes the heating of electrons moving along the edge of the quantum well (see Fig. 3b). Then, the appearance of photoconductance peaks observed when the Fermi level falls between the Dirac point and the bottom of the conduction band finds a natural explanation, because the probability and, thus, the concentration of these metallic electron droplets increase as the Fermi level approaches the bottom of the conduction band. The Drude character of the absorption is corroborated by the fact that the magnitudes of the photoconductance at wavelengths of 184 and 118 μm are related as λ^2. The suggested mechanism of photoconductance also explains the absence of a peak under the conditions where the Fermi level is located near the valence band. Evidently, in this case, there are only hole droplets, and the hole mobility is much lower than that of electrons. Thus, as was already mentioned in the discussion of the valence-band photoconductance, the Drude absorption falls abruptly, which is accompanied by a corresponding drop in the photoconductance.

Figure 3c shows the results of photoconductance measurements in magnetic fields up to 1.5 T. Evidently, the magnetic field considerably changes the behavior of the photoconductance: its magnitude increases with the field strength up to 1 T and drops abruptly as the field is further increased to 1.5 T, while the peak shifts and actually appears within the conduction band. This behavior also supports the proposed mechanism of the "quasi-bulk" Drude absorption of terahertz radiation followed by the heating of one-dimensional electrons, because, in this range of magnetic fields, there should be almost no effect of the field on the character and the spectrum of edge states [19]. The data shown in Fig. 3c suggest that the peak of this absorption occurs in the vicinity of the magnetic field of 1 T, which corresponds to the cyclotron mass equal to $m_n = 0.01m_0$. A similar picture was observed for other samples under study. The above value agrees well with the calculations of the effective mass at the bottom of the conduction band in 8-nm-thick quantum wells [20]. Thus, the data on terahertz photoconductance confirm the existence of metallic droplets extensively interacting with the edge states.

We are grateful to S.N. Artemenko, A.V. Chaplik, and M.V. Entin for their interest in this study and useful discussions. This work was supported by the Russian Foundation for Basic Research (project nos. 13-02-12148, 14-02-01246, and 14-02-31631), the Russian Academy of Sciences (project no. 24.11), the Ministry of Education and Science of the Russian Federation, and the Deutsche Forschungsgemeinschaft (Japanese–German joint research unit FOR 1483).

REFERENCES

1. M. Z. Hasan and C. L. Kane, Rev. Mod. Phys. **82**, 3045 (2010).
2. X.-L. Qi and S.-C. Zhang, Rev. Mod. Phys. **83**, 1057 (2011).
3. M. König, S. Wiedmann, C. Brüne, A. Roth, H. Buhmann, L. W. Molenkamp, X.-L. Qi, and Sh.-Ch. Zhang, Science **318**, 766 (2007).
4. A. Roth, C. Brune, H. Buhmann, L. W. Molenkamp, J. Maciejko, X.-L. Qi, and Sh.-Ch. Zhang, Science **325**, 294 (2009).
5. G. M. Gusev, Z. D. Kvon, O. A. Shega, N. N. Mikhailov, S. A. Dvoretsky, and J. C. Portal, Phys. Rev. B **84**, 121302(R) (2011).
6. G. M. Gusev, E. B. Olshanetsky, Z. D. Kvon, N. N. Mikhailov, and S. A. Dvoretsky, Phys. Rev. B **87**, 081311(R) (2013).
7. G. M. Gusev, A. Levin, Z. D. Kvon, N. N. Mikhailov, and S. A. Dvoretsky, Phys. Rev. Lett. **110**, 076805 (2013).
8. Z. D. Kvon, E. B. Olshanetsky, D. A. Kozlov, E. G. Novik, N. N. Mikhailov, and S. A. Dvoretsky, J. Low Temp. Phys. **37**, 202 (2011).
9. J. Karch, P. Olbrich, M. Schmalzbauerb C. Zoth, C. Brinsteiner, M. Fehrenbacher, U. Wurstbauer, M. M. Glazov, S. A. Tarasenko, E. L. Ivchenko, D. Weiss, J. Eroms, R. Yakimova, S. Lara-Avila, S. Kubatkin, and S. D. Ganichev, Phys. Rev. Lett. **105**, 227402 (2010).
10. S. D. Ganichev, E. L. Ivchenko, and W. Prettl, Physica E **14**, 166 (2002).
11. E. Ziemann, S. D. Ganichev, I. N. Yassievich, V. I. Perel, and W. Prettl, J. Appl. Phys. **87**, 3843 (2000).
12. G. M. Gusev, E. B. Olshanetsky, Z. D. Kvon, O. E. Raichev, N. N. Mikhailov, and S. A. Dvoretsky, Phys. Rev. B **88**, 195305 (2013).
13. B. A. Bernevig, T. L. Hughes, and S.-C. Zhang, Science **314**, 1757 (2006).
14. O. E Raichev, Phys. Rev. B **85**, 045310 (2012).
15. S. N. Artemenko and V. O. Kaladzhyan, JETP Lett. **97**, 82 (2013).
16. G. M. Gusev, E. B. Olshanetsky, Z. D. Kvon, et al., Phys. Rev. B **89** (2014).
17. J. I. Vayrynen, M. Goldstein, and L. I. Glazman, Phys. Rev. Lett. **110**, 216402 (2013).
18. M. König, M. Baenninger, A. G. F. Garcia, N. Harjee, B. L. Pruitt, C. Ames, Ph. Leubner, Ch. Brüne, H. Buhmann, L. W. Molenkamp, and D. Goldhaber-Gordon, Phys. Rev. X **3**, 021003 (2013).
19. B. Scharf, A. Matos-Abiague, and J. Fabian, Phys. Rev. B **86**, 075418 (2012).
20. M. S. Zholudev, Candidate's Dissertation (Nizhni Novgorod, 2013).

Translated by M. Skorikov